

## Article

# Characteristics and Effects of Laminae on a Cretaceous Reservoir in the Bozi–Dabei Area of the Tarim Basin, China

Wenhui Zhu \*, Tao Mo, Changchao Chen, Chunlei Hu, Cuili Wang, Chaoqun Shi, Lingling Shi and Pengzhen Li

Research Institute of Exploration and Development, PetroChina Tarim Oilfield Company, Korla 841000, China  
\* Correspondence: zhuwenhui08@126.com

**Abstract:** Reservoir heterogeneity is an important factor in oil and gas exploration and development. It has guiding significance for favourable target optimization because it helps clarify the formation and development characteristics of laminae: thin, alternating layers of sediment deposited in a repeating pattern in Cretaceous sandstone reservoirs. Reservoir heterogeneity is higher when laminae are densely distributed. For example, laminae have a significant influence on reservoir properties in the Kelasu structural belt in the Bozi–Dabei area, Tarim Basin, China, where oil and gas wells have very low productivity. Hence, this study attempts to develop a classification scheme based on laminae to identify how they influence reservoir properties. Based on an analysis of cores, thin section and logging imaging data, laminae in this area can be classified into three types: magnetite-enriched, iron-stained argillaceous-enriched, and grain-size change. Results show that magnetite-enriched and iron-stained argillaceous-enriched laminae are well-developed in the BZ1 and DB10 well areas in northern Bozi. They have much lower porosity compared to a non-laminae reservoir and their lateral permeability is greater than vertical permeability. Grain-size change laminae are well-developed in the southern Bozi region. For the laminated reservoirs, increasing the length of the perforation interval and the perforation density using sand or acid fracturing is an effective method for communicating with the vertical reservoir layers, improving permeability, and increasing single-well production.

**Keywords:** Kelasu structural belt; Bozi–Dabei area; Cretaceous reservoir; iron-stained argillaceous-enriched laminae; characteristics of laminae; reservoir heterogeneity



**Citation:** Zhu, W.; Mo, T.; Chen, C.; Hu, C.; Wang, C.; Shi, C.; Shi, L.; Li, P. Characteristics and Effects of Laminae on a Cretaceous Reservoir in the Bozi–Dabei Area of the Tarim Basin, China. *Processes* **2023**, *11*, 2472. <https://doi.org/10.3390/pr11082472>

Academic Editor: Qingbang Meng

Received: 25 June 2023

Revised: 30 July 2023

Accepted: 7 August 2023

Published: 17 August 2023



**Copyright:** © 2023 by the authors. Licensee MDPI, Basel, Switzerland. This article is an open access article distributed under the terms and conditions of the Creative Commons Attribution (CC BY) license (<https://creativecommons.org/licenses/by/4.0/>).

## 1. Introduction

The Kelasu structural belt in the north of the Tarim Basin is the main gas source for China's West–East Natural Gas Transmission Project. The western Bozi–Dabei area is the main region for increasing natural gas reserves and production. The exploration target in this area is the Cretaceous Bashijiqike and Baxigai formations, an ultra-deep ultra-low porosity and ultra-low permeability sandstone reservoir at least 6000 m deep. It has mostly faulted-anticline and anticline structure gas reservoirs. It is generally believed that the structural high part is the low stress area, which has developed natural fractures, good physical properties, and high potential for oil and gas production. In the oil and gas exploration and development of Bozi–Dabei area, the productivity of some wells in the high structural position is inferior to those in the low structural position. Take BZ 102 well for example: it is located in the eastern part of the Bozi 1 structure and characterized by a high structural position, high porosity (6–11%), and coarse sandstone particles, with medium sandstone accounting for more than 60%. The physical properties of the reservoir are better than those of the adjacent high-production wells, but its tested output after reconstruction is low: daily gas production is less than  $10 \times 10^4 \text{ m}^3/\text{d}$ . For these wells, the laminae are usually densely developed. Besides the influence of the structure, the sedimentary environment and structure also have great influence on reservoir quality, and reservoir heterogeneity is strong: a hot topic in oil and gas exploration in recent years. Predecessors have classified the types of reservoir heterogeneity according to different

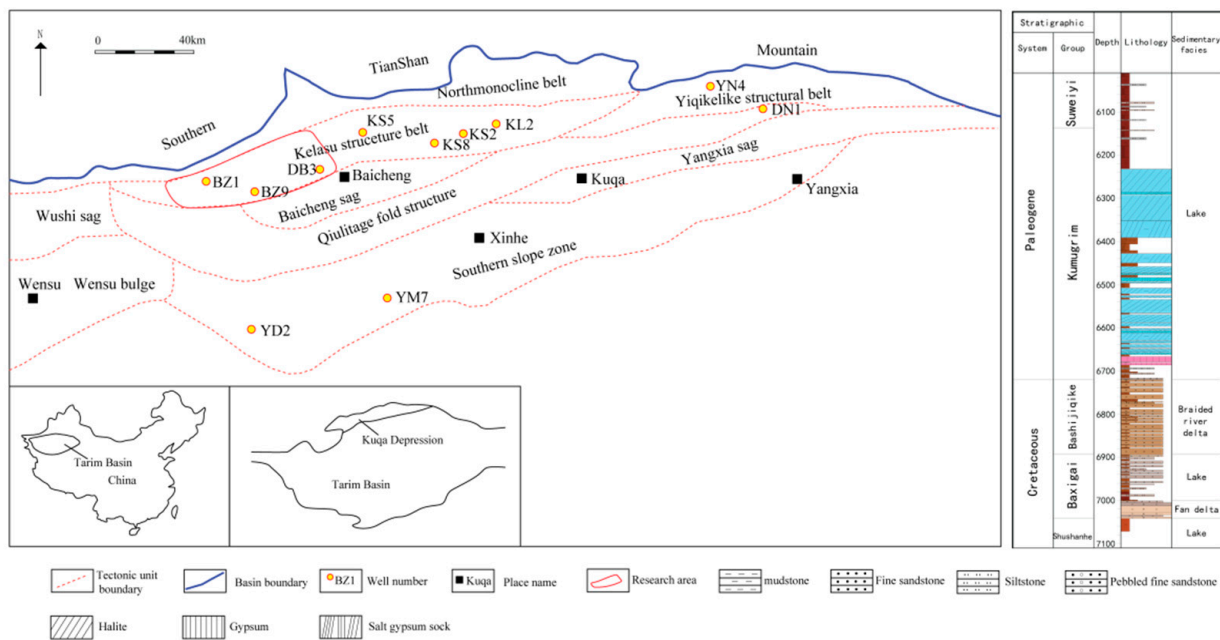
research scales [1–7]. This paper will study the interlayer heterogeneity in the Bozi–Dabei area from the perspective of laminae and microstructures.

The study of laminae was first recorded in 1862 by a Swedish geologist as “hvarfig lera”, meaning “circulatory layer” [8]. Laminae deposits, often measured in years, can be applied to a lot of research, such as reconstructing paleoclimates [9], tracking ecosystem responses to climate change [10], assessing human environmental impacts [11], determining intervals between volcanic eruptions and floods [12,13], assessing regional hazards, and, most importantly, enabling accurate dating on absolute calendar year timescales [14]. Laminae are the most basic and smallest constituent unit of stratification. The thickness of a single layer is usually less than 1 mm, and the maximum is several centimetres [15,16]. The thickness positively correlates with the hydrodynamic strength and material supply abundance [17]. With deeper oil and gas exploration and development, the study of laminae has received more and more attention, mainly for fine-grained sedimentary rocks such as carbonate and shale [18–23]. It is believed that shale rich in silty laminae usually indicates a good shale gas production layer [24], and silty laminae are closely related to horizontal fractures [25], which may play a role in the formation of shale gas transport and storage. Laminated muddy limestone is considered to have good hydrocarbon generation potential and is also a good reservoir rock [19].

However, there are few related studies on laminae in sandstone, especially from the standpoint of microstructures and reservoir physical property. Why can high oil and gas production not be achieved in sandstone reservoirs with densely developed laminae? What is the composition, genesis, distribution of the laminae, and their effect on the reservoir? This paper analyzed lamina characteristics in the Bozi–Dabei area by building a scheme to classify laminae and evaluate their influence on reservoir physical properties by using cores, thin sections, and logging imaging data. The results of this study are also applicable to the oil and gas exploration and development in sandstone reservoirs with dense laminae distribution in other areas.

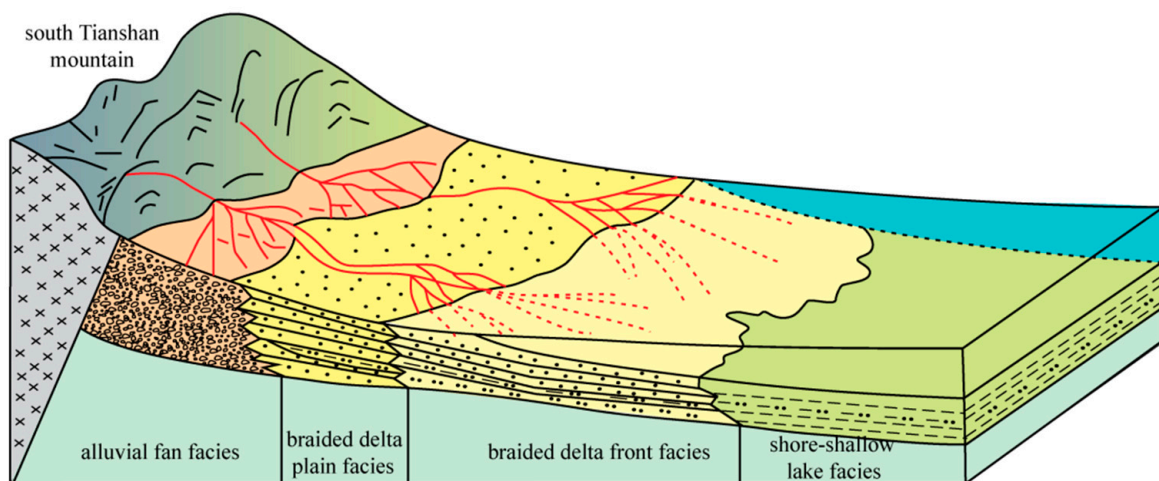
## 2. Geological Settings

The Kuqa depression began to develop from the late Hercynian period and has experienced multiple tectonic movements. It is a Cenozoic rejuvenated foreland basin superimposed on the Triassic peripheral foreland basin, which was developed based on the Palaeozoic passive continental margin [26,27]. The Kelasu structural belt is the thrust structure in the northern Kuqa Depression of the Tarim Basin [28,29], which is divided into four sections from west to east: Awate, Bozi, Dabei, and Keshen [30,31]. The Bozi–Dabei section of the Kelasu structural belt (Figure 1) is the main site of gas production in the “14th Five-Year Plan” of the Tarim Oilfield [32] because of its favourable petroleum accumulation. The hydrocarbon source rocks of the Triassic and Jurassic periods are, respectively, lacustrine mudstones and coal-bearing strata, with large thickness, wide distribution range, and higher maturity [33]. The Cretaceous Bashijiqike and Baxigai formations are the main exploration targets for oil and gas. The lithology of the formation is mainly fine-medium lithic feldspathic sandstone and feldspathic detritus sandstone, interbedded with thin layers of mudstone, silty mudstone, and siltstone. The sedimentary facies are mainly braided river delta and fan delta front deposition, which are vertically characterized by the overlapping of a multi-stage underwater distributary channel and mouth bar sand bodies [34,35]. The reservoir thickness is between 100 and 320 m. Thick salt and gypsum layers of Eocene are the high-quality regional seal. The maximum thickness is above 4000 m. The Triassic and Jurassic source rocks, Cretaceous reservoir, and Eocene cap form an excellent source–reservoir–cap rock combination, which is favourable for the formation of large gas fields. Laminae are widely developed in the sandstone of Cretaceous Bashijiqike and Baxigai formations [36].



**Figure 1.** Division of structural units in Kuqa Depression and the location of research area.

Since Mesozoic, the Kuqa depression presents the pattern of “North Mountain and South Basin”, influenced by multiple stages of composite uplift of the southern Tianshan orogen [29]. This ancient geographic feature determines the distribution of Cretaceous sedimentary facies and skeletal sand bodies. As a foreland basin [37], the ancient topography determines the paleocurrent direction which is from north to south in the Bozi area, with the southern Tianshan mountains as the source area. During the early Bashiji qike formation sedimentation, the study area experienced strong tectonic activities with rapid uplift of the orogenic belt, and significant elevation difference between sedimentary and source area, which led to a relatively steep alluvial fan–fan delta–shallow lake sedimentary system (Figure 2) with relatively low sedimental maturity. Multiple alluvial fans developed along the northern margin of the basin, connected with each other in the plane, and the sedimentary facies exhibited changed significantly in the north–south direction. During the middle–late of the Bashiji qike formation sedimentation, tectonic activities became weak, and the uplift of the orogenic belt was slow. With the process of infilling and levelling, the ancient topography became flatter [38–40].



**Figure 2.** Model of sedimentary facies in Kuqa Depression.




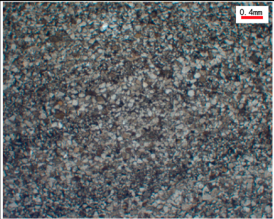
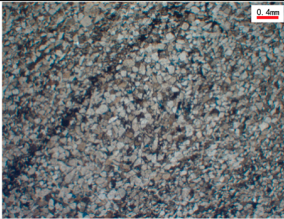
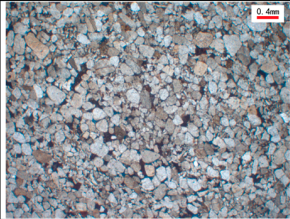


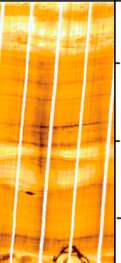
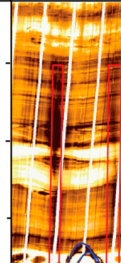
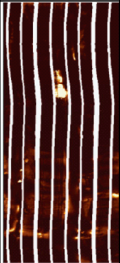
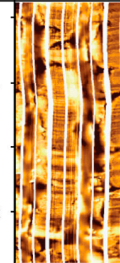
### 3. Data and Method

In the study, 51 representative wells were selected and their cores (in total 695 m) were observed and measured to analyse the laminae characteristics. Samples were selected from the cores with laminae and 112 casting thin sections were made. The microscopic characteristics of laminae in thin sections were observed under microscope and their components were identified. At the same time, the cores were also used to identify and calibrate the laminae on the Formation MicroScanner Image (FMI) logging imaging. Based on these analysis, the FMI imaging logging data of 18 wells without core data were used to assist the identification of laminae. The logging interpretation data of 69 wells and the full-diameter physical property analysis data of 23 wells were used to analyse the influence of laminae on reservoir physical properties.

### 4. Results

#### 4.1. Laminae Classification and Their Characteristics

Based on the analysis of cores, cast thin sections, and logging imaging data, laminae in the Bozi–Dabei area were classified into three types: iron-stained argillaceous-enriched, magnetite-enriched, and grain-size change laminae based on colour, mineral composition, and grain size distribution (Figure 3).

| Laminae type                | Iron stained argillaceous enrichment laminae  |              | Magnetite enrichment laminae   |  | Grain size change laminae   |   |   |              |   |
|-----------------------------|---|--------------|--|--|---|---|---|--------------|---|
| Core                        |   |              |   |  |   |   |   |              |   |
| Casting thin section        |    |              |  |  |  |   |   |              |   |
| Imaging logging             | Still picture   | Depth (m)    | Dynamic picture  | Still picture  | Depth (m)   | Dynamic picture   | Still picture   | Depth (m)    | Dynamic picture   |
|                             |    | 7276<br>7277 |   |   | 6848<br>6849  |  |    | 7221<br>7222 |  |
| Standard for classification | The cores show brown and dark brown stripes. The matrix composition is mainly iron stained argillaceous. It is dark stripe in the location of laminae development in the FMI imaging logging. |              |  | The cores show dark black stripes which are enriched in magnetite. It is black stripe in the location of laminae development in the FMI imaging logging. |   |   | The cores show no obvious color and composition variation. Fine sand and medium coarse sand are distributed in parallel with each other. The characteristic of light and dark bands is obvious with good continuity in the FMI imaging logging. |              |   |

**Figure 3.** Characteristic of different types of laminae in core, thin section and imaging logging.

For reservoirs with iron-stained argillaceous-enriched laminae, the cores show brown and dark brown stripes. The thickness of single-layer laminae varies from 0.2 mm to 1.5 mm with an average of 0.5 mm. The lithology is mainly fine sandstone and the laminae are well-developed near the mudstone and mud-gravel sandstone. In the cast thin sections (Figure 3), silty-fine sand and iron-stained argillaceous assemble as thin layers distributed

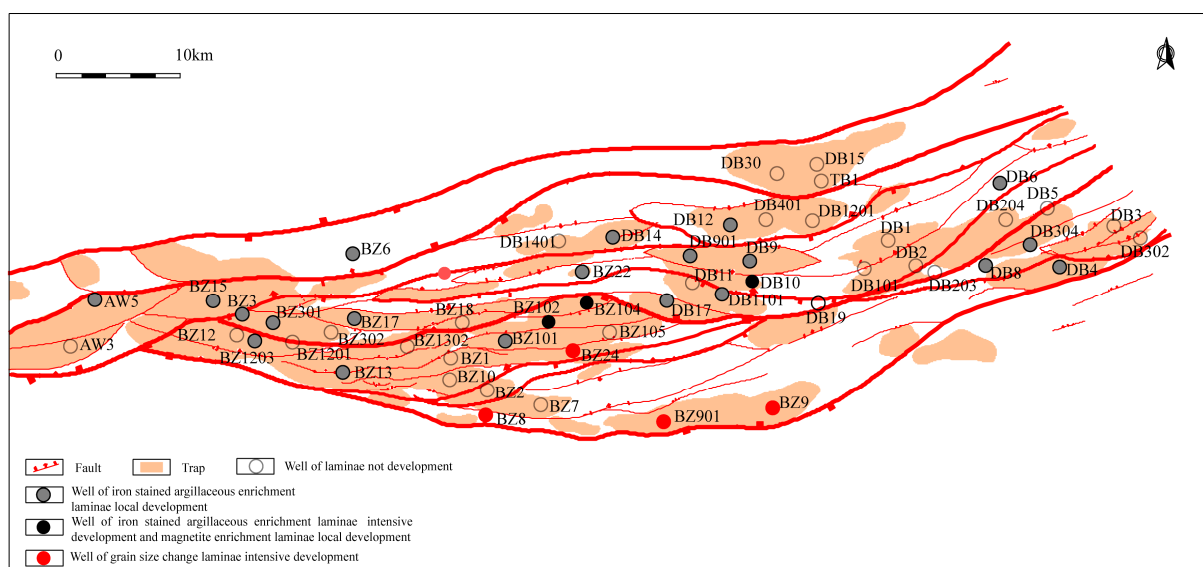
in well-developed areas of the laminae, with a high matrix content and fine grains. The matrix composition is mainly iron-stained argillaceous, with the colour of brown and dark brown, which is different in mudstone. In the FMI imaging logging, the laminae show dark stripes, and the dark stripes become bold in the location of mud gravel development.

For reservoirs with magnetite-enriched laminae, the cores show dark black stripes. The thickness of a single-layer lamina varies from 0.2 mm to 2 mm with an average of 0.8 mm. The lithology is consistent with iron-stained argillaceous-enriched laminae, except that there are a lot of opaque, no cleavage, granular, or irregular dark minerals. These dark minerals can be attracted by a magnet. With the help of the microscope, the dark minerals are identified as magnetite. In the FMI imaging logging, the laminae have higher electrical conductivity and show black stripes (Figure 3).

For reservoirs with grain-size change laminae, the cores show no obvious colour and composition variation. The thickness of a single layer varies from 0.5 mm and 5 mm with an average of 1.5 mm. The lithology is mainly coarse, medium-coarse and fine sand, which are distributed in parallel. Due to the presence of coarse particles, fine sand laminae are compacted tightly and there are rarely pores between grains. However, in the medium-coarse sand laminae, there are primary and secondary pores. In the FMI imaging logging, the light and dark bands are obvious with good continuity (Figure 3).

#### 4.2. Plane Distribution of Laminae

According to the core, thin section, and FMI logging imaging analysis, laminae are widely developed in the Cretaceous sandstone reservoir in the Bozi–Dabei area, but there are only a few wells with a dense distribution of laminae in the entire target horizon. Iron-stained argillaceous-enriched laminae are mainly distributed in BZ 1, DB 10, and the northern well areas (Figure 4), which are densely developed around the wells of BZ 102, BZ 104, and DB 10, but locally developed in other wells according to cores and FMI logging imaging analysis. The magnetite-enriched laminae are well-developed in the entire target horizon only a few wells including BZ 102, BZ 104, and DB 10. The grain-size change laminae are mainly developed in the southern Bozi area including wells BZ 24, BZ 8, and BZ 901 (Figure 4).



**Figure 4.** Plane distribution of different types of laminae in the Bozi–Dabei area.

#### 4.3. Vertical Distribution of Laminae

The magnetite-enriched and iron-stained argillaceous-enriched laminae are mainly developed in the upper of the normal depositional cycle with fine grain size and high argillaceous content. The GR curves are often represented as a bell-shaped feature in the

upper but a box-shaped feature at the bottom where laminae are undeveloped. The grain-size variation laminae are mainly developed in the middle of the normal depositional cycle with coarse grain size and low argillaceous content. The GR curves are often represented as a high amplitude box-shaped feature.

## 5. Discussion

### 5.1. The Influencing Factors of the Laminae Formation

Previous studies have suggested that the formation of laminae is influenced by various factors, such as climate, lake bottom topography, water properties, the amount of terrestrial debris, and biological processes [41–44]. From the sedimentary facies plan, in the depositional stage of the Bashijiqike formation, the paleocurrent direction in most of the Bozi area was from north to south. However, it was from north to east and south in the area of the Bozi 8 and Bozi 9 wells. In the Bozi 12 well area, the paleocurrent is from south to north. The sedimentary facies near the southern Tianshan Mountain is braided river delta plain and it gradually becomes braided river delta front southward (Figure 5). Stable heavy minerals in the study area are mainly composed of magnetite, hematite, ilmenite, zircon, garnet, tourmaline, etc., with magnetite content being the highest, accounting for about 60%. From the comprehensive analysis of sedimentary facies and heavy minerals, it is believed that with the increase in transport distance, the energy of the water body weakens, the flow rate slows down, the content of stable heavy minerals and fine-grained sediment increases, resulting in the increase in iron-stained argillaceous content and the layer distribution of magnetite in the Bozi 1, Dabei 10, and Dabei 6 well areas at the braided river delta front. The content of iron-stained argillaceous is high, and the magnetite-enriched layers are well-developed. In the southern Bozi–Dabei area, the sedimentation of the Cretaceous Bashijiqike formation is influenced by the paleocurrent from north to the south and east (Figure 5), with a coarser grain size, sufficient grain sorting, low argillaceous content, and alternating coarse and fine-grained sedimentation, resulting in the development of grain size change laminae in the southern Bozi area.

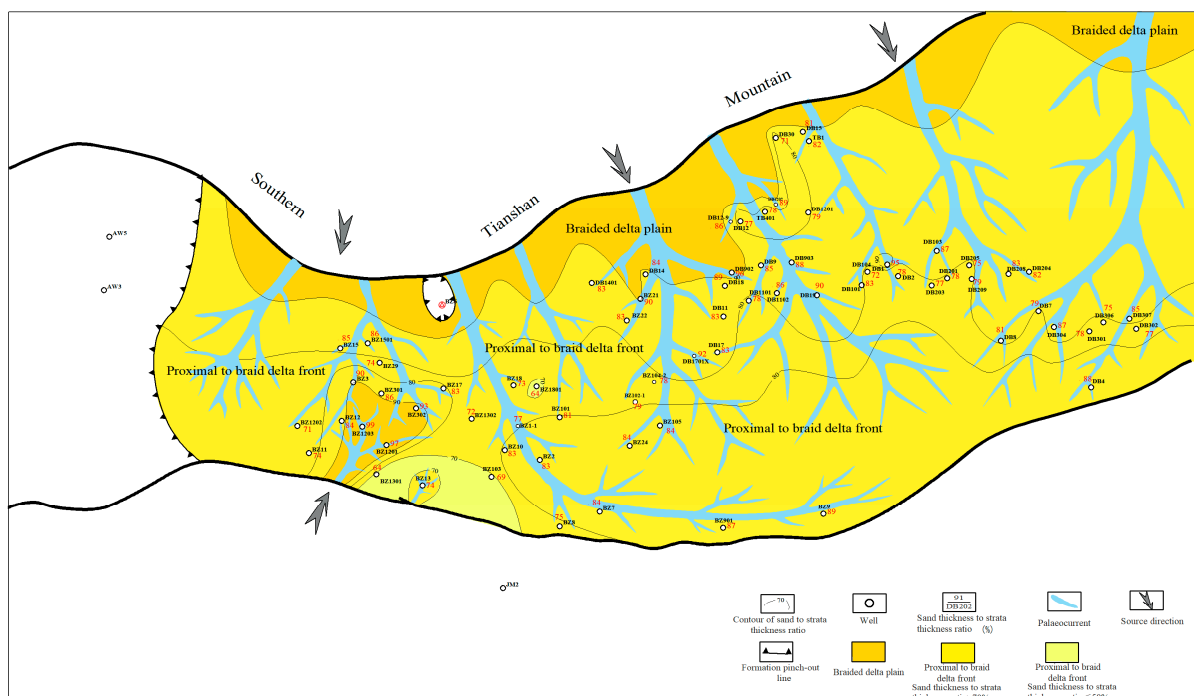
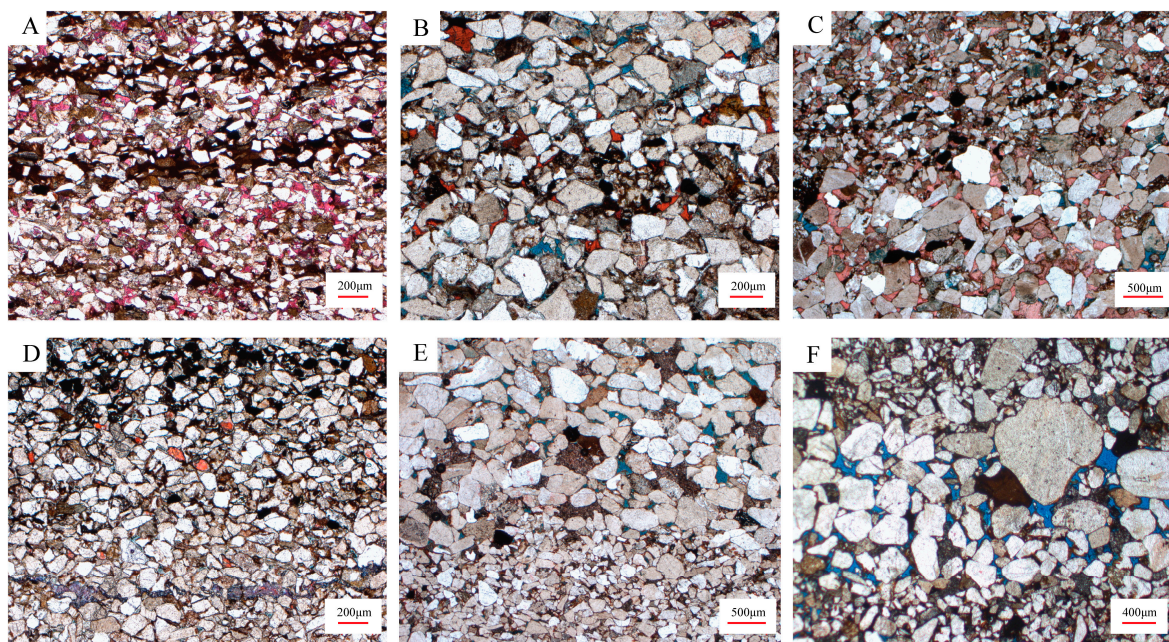


Figure 5. Sedimentary facies of the Cretaceous Bashijiqike Formation in the Bozi–Dabei area.

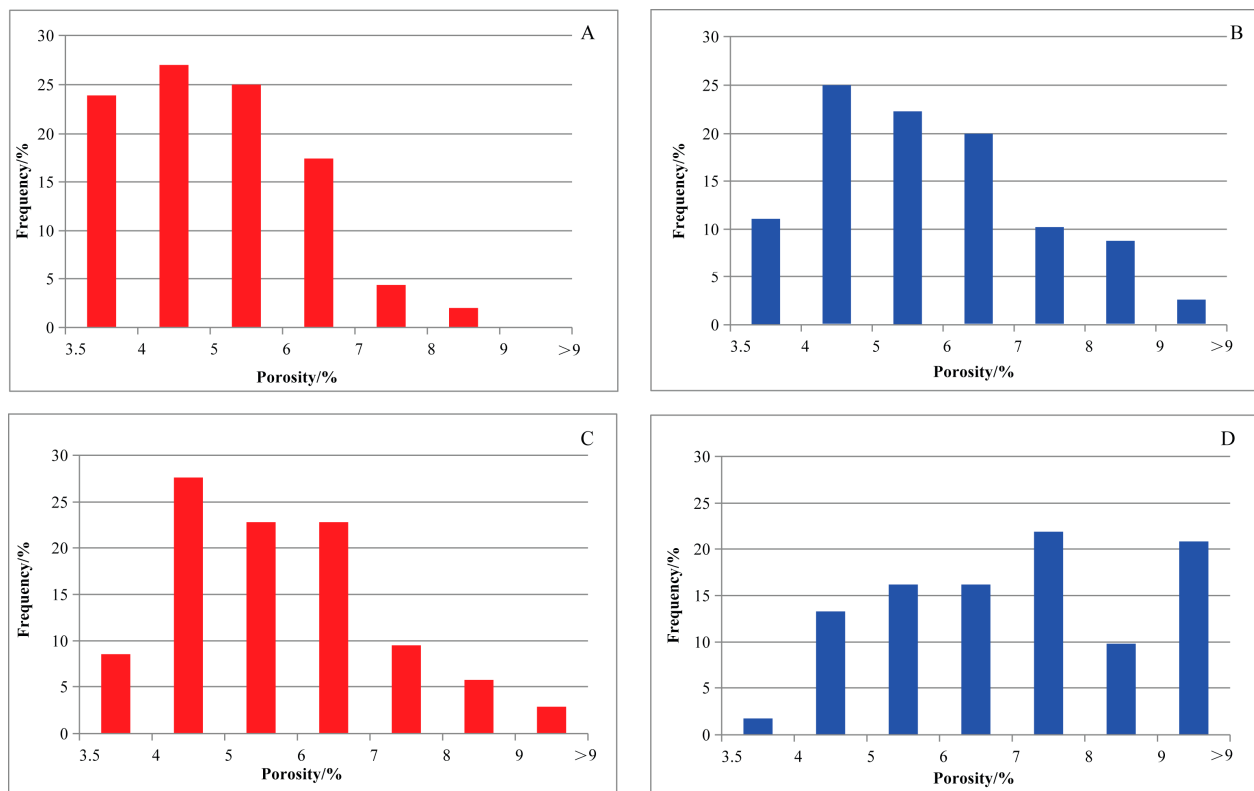
### 5.2. Effects of Laminae on Reservoir Properties

Analysis of 112 cast thin sections from 32 wells in the Bozi–Dabei area shows that the lithology of the reservoir with iron-stained argillaceous-enriched laminae is mainly composed of fine and medium sandstone, with a significant increase in iron-stained argillaceous in the filling materials, which are distributed in thin layers and intermittently parallel to the bedding (Figure 6A–C). The reservoirs always have a strong cementation and low porosity. The magnetite-enriched laminae are similar to the iron-stained argillaceous-enriched laminae, with an increased content of magnetite, which is accumulated and distributed in thin layers (Figure 6C,D). For the reservoirs iron-stained argillaceous-enriched and magnetite-enriched laminae undeveloped, their grain size is relatively coarse, mainly composed of fine to medium sandstone, mainly cemented by calcite, with a small number of intergranular pores, intergranular dissolution pores, and intragranular dissolution pores, and the surface pore rate is obviously higher than that with laminae developed. The grain-size change laminae show a laminated distribution of very fine sand, fine sand, and medium-coarse sand under the microscope, with particles arranged in an oriented manner. The filling materials are mainly composed of iron-stained argillaceous and calcite. A small number of primary intergranular pores, intergranular dissolution pores, intragranular dissolution pores, and clay micropores can be seen in the rock, mainly distributed in the medium-coarse-grained laminae (Figure 6E,F).



**Figure 6.** Thin section characteristics of different types of laminae. (A) BZ13 well, 7005.02 m, iron-stained argillaceous-enriched laminae; (B) BZ22 well, 6279.38 m, iron-stained argillaceous-enriched laminae; (C) AW5 well, 3203.9 m, iron-stained argillaceous-enriched laminae and magnetite-enriched laminae; (D) DB6 well, 6861.7 m, magnetite-enriched laminae; (E) BZ24 well, 7227.65 m, grain-size change laminae; (F) BZ9 well, 7680.3 m, grain-size change laminae.

Several wells were selected to analyse the effects of laminae on the reservoir's porosity. It was found that the logging interpretation effective porosity of the reservoirs with iron-stained argillaceous-enriched and magnetite-enriched laminae ranged from 4.0% to 6.0%, with an average of 5.2%, while the effective porosity of the non-laminated reservoirs ranged from 5.0% to 8.0%, with an average of 6.0%. The logging interpretation effective porosity of the reservoirs with grain-size change laminae ranged from 4.0% to 7.0%, with an average of 5.8%, while the effective porosity of the non-laminated reservoir mainly ranged from 6.0% to 9.0%, with an average of 7.1% (Figure 7).

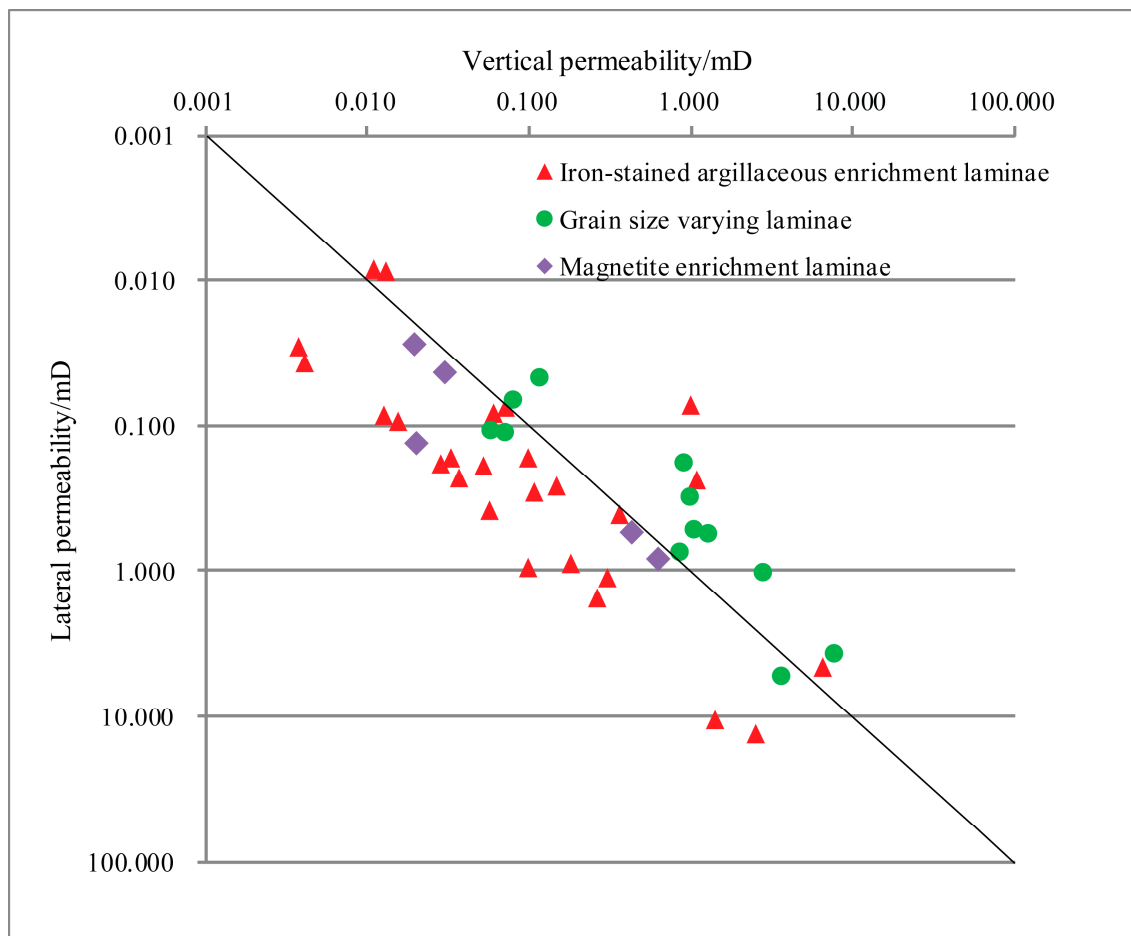


**Figure 7.** Histograms of logging interpretation effective porosity of the laminae and non-laminae reservoir. (A) The logging interpretation effective porosity of the reservoir with iron-stained argillaceous-enriched and magnetite-enriched laminae. (B) The logging interpretation effective porosity of iron-stained argillaceous-enriched and magnetite-enriched laminae undeveloped reservoir. (C) The logging interpretation effective porosity of grain-size change laminated reservoir. (D) The logging interpretation effective porosity of grain-size change laminae undeveloped reservoir.

Overall, the porosity of the reservoir with laminae developed is obviously lower than that of laminae undeveloped. The existence of laminae reduces the reservoir porosity. Additionally, the porosity of the reservoir with grain-size change laminae is higher than the reservoir with iron-stained argillaceous-enriched and magnetite-enriched laminae.

Due to the plan distribution of laminae and its strong vertical heterogeneity, the small plug permeability is not representative which is significantly affected by the sample size. Therefore, the evaluation of permeability is based on the analysis of full-diameter permeability results. For the three types of laminae, core samples from the well-laminated sections were selected for full diameter petrophysical analysis. Analysis shows that the average permeability in the vertical direction of the magnetite-enriched laminae (referred to as vertical permeability, denoted as  $K_{\text{vertical}}$ ) is 0.227 mD, and in the parallel direction of laminae (referred to as lateral permeability, denoted as  $K_{\text{lateral}}$ ) is 0.318 mD, with vertical permeability significantly lower than lateral permeability. The average vertical permeability for the iron-stained argillaceous-enriched laminae is 0.569 mD, and the lateral permeability is 1.372 mD, with vertical permeability significantly lower than lateral permeability. For the laminae with grain-size change, the average vertical permeability is 1.671 mD, and the lateral permeability is 1.378 mD, with little difference between vertical and lateral permeability (Figure 8). Overall, the existence of iron-stained argillaceous-enriched and magnetite-enriched laminae tends to result in lower vertical permeability.

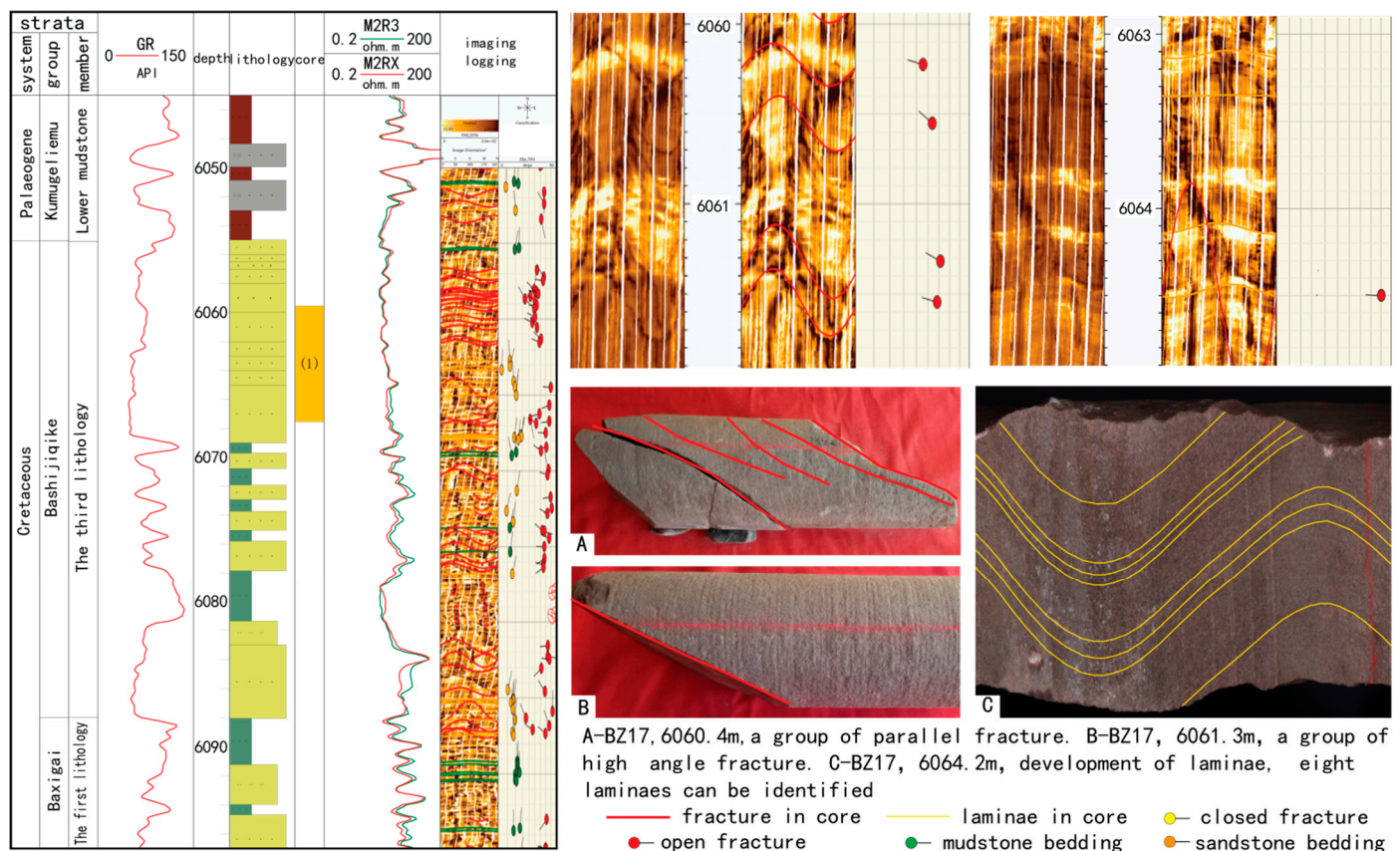




**Figure 8.** The relationship between lateral permeability and vertical permeability of core in different laminae.

### 5.3. Effects of Laminae on Fracture

In rocks, the change in grain size and compositions of debris particles often form a weak stress plane, and the density, size, and dip angle of fractures near the weak stress plane will suddenly change in thick tight sandstone after being subjected to stress [45,46]. The cores shows that fractures in the laminated area often cut in arc or terminate at the laminae bedding plane, and the fracture density in the laminated sections is significantly lower than that in the non-laminated sections. From the FMI logging imaging data, we identified the distribution of fractures. Taking the BZ 17 well as an example, the core is located in the depth of 6059.9–6067.9 m of the Cretaceous Bashijiqi formation. For the core in the depth of 6059.9–6061.9 m, multiple high-angle fractures are developed and the core is broken. The laminae are undeveloped. Four high-angle parallel fractures are identified on the logging image, with an average linear density of two fractures/m. For the core in the depth of 6062.9–6064.9 m, the core is relatively intact, with two high-angle nearly parallel fractures developed. Iron-stained argillaceous-enriched laminae are developed. The logging image shows alternating light and dark stripes, and one high-angle fracture is identified with an average fracture line density of 0.5/m (Figure 9). Overall, the debris particle size, composition, and other changes in the development of lamination are significant, and the elastic properties of rocks change greatly, which to some extent prevents the expansion of fractures in the longitudinal direction.



**Figure 9.** Comprehensive histogram of BZ17 well of Cretaceous Bashijiqike formation and fracture and laminae development characteristics of core. (A) BZ17, 6060.4 m, core, a group of parallel fracture. (B) BZ17, 6061.3 m, core, a group of high angle fracture. (C) BZ17, 6064.2 m, core, eight laminae can be identified.

#### 5.4. Effects of Laminae on Reservoir Reconstruction

A large number of fine-grained laminae in the sandstone reservoir seriously intensify the heterogeneity of the reservoir [47,48]. For the well sections with magnetite-enriched and iron-stained argillaceous-enriched laminae, the reservoir porosity and vertical permeability are significantly reduced, and the fracture size and density are small, resulting in poor vertical connectivity of the reservoir, impairing oil and gas flow, and reducing the exploitation effect. Conventional acid fracturing has limitations: firstly, the vertical extension of artificial fractures is limited due to the existence of laminae, resulting in a small range of reservoir communication. Secondly, the acid fracturing fluid is lost along the laminae bedding plane, which reduces the fracturing effect. Thirdly, there is no obvious impact of acid on the iron-stained argillaceous-enriched laminae and magnetite, affecting the acid fracturing effect. After reservoir reconstruction, the single well productivity cannot be fully released, so it is necessary to increase the length of the perforation interval and perforation density in the laminated sections and choose sand fracturing to maximize the vertical connectivity of the reservoir and improve the flow capacity; thereby, enhancing single well production capacity (Table 1). For well sections with grain-size change laminae, although the fractures are not significantly developed, the reservoir property is good and laminae have little effect on vertical permeability. Most wells can achieve high productivity through conventional testing, with relatively low requirements for reconstruction method. The production capacity will be further improved after sand fracturing.

**Table 1.** Completed testing of representative wells where laminae develop.

| Well  | Completion Testing   | Formation         | Well Section (m) | Nozzle (mm) | Oil Pressure (MPa) | Daily Gas Production (10 <sup>4</sup> m <sup>3</sup> /d) | Daily Oil Production (m <sup>3</sup> /d) | Laminae Type   |
|-------|----------------------|-------------------|------------------|-------------|--------------------|--|--|--|
| BZ102 | routine test         | K <sub>1</sub> bs | 6760–6879        | 3           | 33.80              | 3.23   | 5.54                                     | magnetite-enriched type, iron-stained argillaceous-enriched type |
|       | acid test            |                   |                  | 4           | 38.38              | 10.66  | 10.44                                    |  |
|       | sand fracturing test |                   |                  | 6           | 31.53              | 16.28  | 18.63                                    |  |
| BZ104 | routine test         | K <sub>1</sub> bs | 6757–6850        | 3           | 43.39              | 3.74   | 0.98                                     | magnetite-enriched type  |
|       | sand fracturing test |                   |                  | 7           | 81.29              | 51.19  | 36.38                                    |  |
| BZ9   | routine test         | K <sub>1</sub> bs | 7677–7760.5      | 5           | 86.64              | 22.39  | /  | grain-size variation type  |
|       | sand fracturing test |                   |                  | 8           | 94.35              | 70.55  | 167                                      |  |
| BZ24  | routine test         | K <sub>1</sub> bs | 7320–7390        | 4           | 42.98              | 11.78  | 12.3                                     | grain-size variation type  |
|       | sand fracturing test |                   |                  | 6           | 69.64              | 28.71  | 40.8                                     |  |

## 6. Conclusions

The results show that the development of laminae has a significant effect on reservoir heterogeneity. After an oil and gas well is drilled, it is necessary to identify whether the laminae are developed according to the core, thin section, and logging imaging data. For wells with laminae developed, the type of the laminae should be further identified, and the oil testing method should be further determined according to the laminae type in order to improve the oil and gas productivity. For the Bozi–Dabei area, some understandings are listed as follows:

Laminae are widely developed in Cretaceous sandstone reservoirs in the Bozi–Dabei area and can be divided into three types based on colour, composition, and grain size: magnetite-enriched, iron-stained argillaceous-enriched, and grain-size change laminae. Influenced by the sedimentary environment, the iron-stained argillaceous-enriched and magnetite-enriched laminae are mainly distributed in BZ 1, DB 10, and their northern well areas, while the grain-size change laminae are mainly developed in the southern Bozi area.

The existence of laminae tends to lower the reservoir porosity. The lateral permeability of reservoirs with magnetite-enriched, iron-stained argillaceous-enriched laminae is significantly greater than the vertical permeability while there is little difference between lateral and vertical permeability of reservoirs with grain size change laminae, and the pores are mainly distributed in medium-coarse-grained laminae.

For the laminated reservoirs, increasing the length of perforation interval and perforation density and using sand fracturing or acid fracturing are effective methods for communicating with the vertical reservoirs, improving the flow capacity, and increasing the single-well production.

**Author Contributions:** Writing—original draft preparation, W.Z.; writing—review and editing, T.M.; investigation, C.C. and C.H.; resources, C.W.; data curation, C.S.; validation, L.S. and P.L. All authors have read and agreed to the published version of the manuscript.

**Funding:** This research was funded by the major science and technology project of the China National Petroleum Co., Ltd. (2018E-1801).

**Data Availability Statement:** The data presented in this study are available on request from the corresponding author.

**Conflicts of Interest:** The authors declare no conflict of interest.

## References

1. Pettijohn, F.J. *Sedimentary Rocks*; Harper: New York, NY, USA, 1957.
2. Weber, K.J. Influence of common sedimentary structures on fluid flow in reservoir models. *J. Pet. Technol.* **1982**, *34*, 665–672. [[CrossRef](#)]
3. Matthew, J.P.; Amanda, I.E. Analysis and modeling of intermediate-scale reservoir heterogeneity based on a fluvial point-bar outcrop analog, Williams Fork Formation, Piceance Basin. *AAPG Bull.* **2007**, *91*, 1025–1051.
4. Martyushev, D.A.; Chalova, P.O.; Davoodi, S.; Ashraf, U. Evaluation of facies heterogeneity in reef carbonate reservoirs: A case study from the oil field, Perm Krai, Central-Eastern Russia. *Geoenergy Sci. Eng.* **2023**, *227*, 211814. [[CrossRef](#)]
5. Makarian, E.; Abad, A.B.M.N.; Manaman, N.S.; Mansourian, D.; Elyasi, A.; Namazifard, P.; Martyushev, D. An efficient and comprehensive poroelastic analysis of hydrocarbon systems using multiple data sets through laboratory tests and geophysical logs: A case study in an Iranian hydrocarbon reservoir. *Carbonates Evaporites* **2023**, *38*, 37. [[CrossRef](#)]
6. Galkin, S.V.; Martyushev, D.A.; Osovetsky, B.M.; Kazymov, K.P.; Song, H. Evaluation of void space of complicated potentially oil-bearing carbonate formation using X-ray tomography and electron microscopy methods. *Energy Rep.* **2022**, *8*, 6245–6257. [[CrossRef](#)]
7. Martyushev, D.A.; Ponomareva, I.N.; Chukhlov, A.S.; Davoodi, S.; Osovetsky, B.M.; Kazymov, K.P.; Yang, Y. Study of void space structure and its influence on carbonate reservoir properties: X-ray microtomography, electron microscopy, and well testing. *Marine Petrol. Geol.* **2023**, *151*, 106192. [[CrossRef](#)]
8. Zolitschka, B.; Francus, P.; Ojala, A.; Schimmelmann, A. Varves in lake sediments—A review. *Quat. Sci. Rev.* **2015**, *117*, 1–41. [[CrossRef](#)]
9. Larocque-Tobler, I.; Filipiak, J.; Tylmann, W.; Bonk, A.; Grosjean, M. Comparison between chironomid-inferred mean-August temperature from varved Lake Zabinskie (Poland) and instrumental data since 1896 AD. *Quat. Sci. Rev.* **2015**, *111*, 35–50. [[CrossRef](#)]
10. Randsalu-Wendrup, L.; Conley, D.; Carstensen, J.; Snowball, I.; Jessen, C.; Fritz, S. Ecological Regime Shifts in Lake Kälksjön, Sweden, in Response to Abrupt Climate Change Around the 8.2 ka Cooling Event. *Ecosystems* **2012**, *15*, 1336–1350. [[CrossRef](#)]
11. Lotter, A.; Birks, H. The separation of the influence of nutrients and climate on the varve time-series of Baldeggersee, Switzerland. *Quat. Sci. Rev.* **1997**, *59*, 362–375. [[CrossRef](#)]
12. Corella, J.; Benito, G.; Rodriguez-Lloveras, X.; Brauer, A.; Valero-Garces, B. Annually-resolved lake record of extreme hydro-meteorological events since AD 1347 in NE Iberian Peninsula. *Quat. Sci. Rev.* **2014**, *93*, 77–90. [[CrossRef](#)]
13. Czymzik, M.; Brauer, A.; Dulski, P.; Plessen, B.; Naumann, R.; Grafenstein, U.; Scheffler, R. Orbital and solar forcing of shifts in Mid- to Late Holocene flood intensity from varved sediments of pre-alpine Lake Ammersee (southern Germany). *Quat. Sci. Rev.* **2013**, *61*, 96–110. [[CrossRef](#)]
14. Nakagawa, T.; Gotanda, K.; Haraguchi, T.; Danhara, T.; Yonenobu, H.; Brauer, A.; Yokoyama, Y.; Tada, R.; Takemura, K.; Staff, R. SG06, a fully continuous and varved sediment core from Lake Suigetsu, Japan: Stratigraphy and potential for improving the radiocarbon calibration model and understanding of late Quaternary climate changes. *Quat. Sci. Rev.* **2012**, *36*, 164–176. [[CrossRef](#)]
15. Campbell, C. Lamina, Laminaset, bed and bedset. *Sedimentology* **1967**, *8*, 7–26. [[CrossRef](#)]
16. Lazari, O.; Bohacs, K.; Schieber, J.; Macquakeret, J.; Demko, T. *Mudstone Primer: Lithofacies Variations, Diagnostic Criteria and Sedimentologic-Stratigraphic Implications at Lamina to Bedset Scales*; SEPM Society for Sedimentary Geology: Tulsa, OK, USA, 2015; Volume 12.
17. Xiao, Y. *A Concise Tutorial on Petrology*; Geol Publishing Press: Beijing, China, 2014.
18. Luan, X.; Kong, X.; Zhang, J.; Jiang, L.; Peng, Y.; Cai, Y. Astronomical Forcing of Origins of Eocene Carbonate-bearing Fine-grained Sedimentary Rock in Dongying Sag. *Acta Sedimentol. Sin.* **2022**, 1–21.
19. Zhao, X.Z.; Zhu, J.Q.; Zhang, R.F.; Yu, Z.W.; Wang, J.M.; Guo, Y.J. Characteristics and exploration potential of tight calcilutite-rudstone reservoirs in Shulu sag, Jizhong depression, North China. *Acta Pet. Sin.* **2014**, *35*, 613–622.
20. Yawar, Z.; Schieber, J. On the origin of silt laminae in laminated shales. *Sediment. Geol.* **2017**, *360*, 22–34. [[CrossRef](#)]
21. Xin, B.; Zhao, X.; Hao, F.; Jin, F.; Pu, X.; Han, W.; Xu, Q.; Guo, P.; Tian, J. Laminae characteristics of lacustrine shales from the Paleogene Kongdian Formation in the Cangdong Sag, Bohai Bay Basin, China: Why do laminated shales have better reservoir physical properties? *Int. J. Coal Geol.* **2022**, *260*, 104056. [[CrossRef](#)]
22. Liu, G.; Liu, B.; Huang, Z.; Chen, Z.; Jiang, Z.; Guo, X.; Li, T.; Chen, L. Hydrocarbon distribution pattern and logging identification in lacustrine fine-grained sedimentary rocks of the Permian Lucaogou formation from the Santanghu basin. *Fuel* **2018**, *222*, 207–231. [[CrossRef](#)]
23. Liu, G.; Zhai, G.; Huang, Z.; Zou, Z.; Xia, C.; Shi, X.; Zhou, D.; Zhang, Z.; Chen, C.; Yu, R.; et al. The effect of tuffaceous material on characteristics of different lithofacies: A case study on Lucaogou Formation fine-grained sedimentary rocks in Santanghu Basin. *J. Pet. Sci. Eng.* **2019**, *179*, 355–377. [[CrossRef](#)]
24. Broadhead, R.F.; Kepferle, R.C.; Potter, P.E. Stratigraphic and sedimentologic controls of gas in shale—Example from Upper Devonian of northern Ohio. *AAPG Bull.* **1982**, *66*, 10–27.
25. Lash, G.G.; Engelder, T. An analysis of horizontal microcracking during catagenesis: Example from the Catskill delta complex. *AAPG Bull.* **2005**, *89*, 1433–1449. [[CrossRef](#)]

26. Yu, H.; Qi, J.; Yang, X.; Liu, Q.; Cao, S.; Fan, S.; Sun, T.; Yang, X. The Mesozoic Tectonic Palaeogeographic Analysis in Kuqa Depression of Tarim Basin. *Geol. J. China Univ.* **2016**, *22*, 657–669.
27. Wang, K.; Yang, H.; Li, Y.; Zhang, R.; Ma, Y.; Wang, B.; Yu, C.; Yang, Z.; Tang, Y. Geological characteristics and exploration potential of the northern tectonic belt of Kuqa depression in Tarim Basin. *Acta Pet. Sin.* **2021**, *42*, 885–905.
28. Han, Y.; Gu, Y.; Liu, J.; Shang, G.; Wang, B.; Lv, R. Tectonic Origin and the Prospect of Oil Gas in West Kelasu Structural Belt: A Case Study of Awat Segment. *Nat. Gas Geosci.* **2016**, *27*, 2160–2168.
29. Yu, H.; Qi, J.; Yang, X.; Sun, T.; Liu, Q.; Cao, S. Analysis of Mesozoic Prototype Basin in Kuqa Depression, Tarim Basin. *Xinjiang Pet. Geol.* **2016**, *37*, 644–666.
30. Xu, Z.; Xie, H.; Li, Y.; Lei, G.; Wu, C.; Neng, Y. Characteristics and Controlling Factors of the Subsalt Differential Structure in the Kelasu Structural Belt, Kuqa Depression. *Nat. Gas Geosci.* **2012**, *23*, 1034–1038.
31. Wang, B.; Lei, G.; Wu, C.; Mo, T.; Zhou, P.; Shang, J.; Xie, Y.; Li, M. Division and sedimentary models for the Palaeogene gypsum mudstones in the Kuqa depression, Xinjiang. *Sediment. Geol. Tethyan Geol.* **2016**, *36*, 60–65.
32. Tian, J.; Yang, H.; Wu, C.; Mo, T.; Zhu, W.; Shi, L. Discovery of Well Bozi 9 and ultra-deep natural gas exploration potential in the Kelasu tectonic zone of the Tarim Basin. *Nat. Gas Ind.* **2020**, *40*, 11–19.
33. Wang, Z. Formation mechanism and enrichment regularities of Kelasu subsalt deep large gas field in Kuqa Depression, Tarim Basin. *Nat. Gas Geosci.* **2014**, *25*, 153–166.
34. Liu, C.; Zhang, H.; Han, B.; Zhang, R.; Chen, G. Reservoir Characteristics and Control Factors of Deep-Burial Clastic Rocks in Dabei Zone of Kuche Sag. *Nat. Gas Geosci.* **2009**, *20*, 504–512.
35. Zhang, R.; Liu, C.; Yang, H.; Zhang, H.; Wang, J.; Zeng, Q. Characteristics and Exploration Potential of Ultra-Deep Cretaceous Reservoir in Kuqa Depression, Tarim Basin. *Xinjiang Pet. Geol.* **2016**, *37*, 423–429.
36. Yang, H.; Li, Y.; Tang, Y.; Lei, G.; Zhou, L.; Zhou, P. Discovery of Kelasu Subsalt Deep Large Gas Field, Tarim Basin. *Xinjiang Pet. Geol.* **2019**, *40*, 12–20.
37. Chen, G.; Huang, Z.; Zhang, H.; Zhang, R.; Yan, X. Provenance analysis of clastic rocks in the Cretaceous Bashijiqike formation at Kuqa depression. *Nat. Gas Geosci.* **2012**, *23*, 1025–1033.
38. Ma, Y.; Zhang, R.; Tang, Y.; Chen, G.; Mo, T.; Wang, J.; Xie, B. Lithofacies Paleogeography of Cretaceous Bashijiqike Formation in Kuqa Depression, Tarim Basin. *Xinjiang Pet. Geol.* **2016**, *37*, 249–256.
39. Xiao, J.; Lin, C.; Liu, J. Depositional Palaeogeography of Cretaceous of Kuqa Depression in Northern Tarim Basin. *Geoscience* **2005**, *19*, 253–260.
40. Zhou, P.; Xie, Y.; Neng, Y.; Sun, D.; Wang, B.; Zhang, X. Dark Laminae of Bashijiqike Formation and Well Logging Response in Bozi Area of Kuqa Depression, Tarim Basin. *Xinjiang Pet. Geol.* **2016**, *37*, 286–290.
41. Wang, M.; Lu, J.; Zuo, Z.; Li, H.; Wang, B. Characteristics and dominating factors of lamellar fine-grained sedimentary rocks: A case study of the upper Es4 member-lower Es3 member, Dongying Sag, Bohai Bay Basin. *Petro Geol Exp.* **2018**, *40*, 470–478.
42. Li, T.; Zhu, R.; Bai, B.; Wang, C.; Li, T. Characteristics and Research Significance of Fine Lacustrine Sedimentary Rock Laminations of Xiagou Formation in Qingxi Depression of Jiuquan Basin. *China Pet. Explor.* **2015**, *20*, 38–47.
43. Bai, C.; Yu, B.; Liu, H.; Xie, Z.; Han, S.; Zhang, L. The genesis and evolution of carbonate minerals in shale oil formations from Dongying depression, Bohai Bay Basin. *Int. J. Coal Geol.* **2018**, *189*, 8–26. [[CrossRef](#)]
44. Einsele, G.; Seilacher, A. *Cyclic and Event Stratification*; Springer: Berlin/Heidelberg, Germany, 1982; p. 536.
45. Julia, F.; Robert, M.; Jon, H. Natural fractures in the Barnett Shale and their importance for hydraulic fracture treatments. *AAPG Bull.* **2007**, *91*, 603–622.
46. Swanson, S. Lithostratigraphic controls on bedding-plane fractures and the potential for discrete groundwater flow through a siliciclastic sandstone aquifer, southern Wisconsin. *Sediment. Geol.* **2007**, *197*, 65–78. [[CrossRef](#)]
47. Bahlani, A.M.; Babadagli, T. SAGD laboratory experimental and numerical simulation studies: A review of current status and future issues. *J. Pet. Sci. Eng.* **2009**, *68*, 135–150. [[CrossRef](#)]
48. Swapan, K.D.; Roger, M.B. Mechanism of the vapor extraction process for heavy oil and bitumen. *J. Pet. Sci. Eng.* **1998**, *21*, 43–59.

**Disclaimer/Publisher's Note:** The statements, opinions and data contained in all publications are solely those of the individual author(s) and contributor(s) and not of MDPI and/or the editor(s). MDPI and/or the editor(s) disclaim responsibility for any injury to people or property resulting from any ideas, methods, instructions or products referred to in the content.